

# Ocean contribution to co-seismic crustal deformation and geoid anomalies: application to the 2004 December 26 Sumatra-Andaman earthquake

D.B.T. Broerse<sup>a</sup>, L.L.A. Vermeersen<sup>a</sup>, R.E.M. Riva<sup>a,b</sup>, W. van der Wal<sup>a</sup>

<sup>a</sup>*Faculty of Aerospace Engineering, Delft University of Technology, Kluyverweg 1, 2629 HS Delft, The Netherlands*

<sup>b</sup>*Faculty of Geosciences, Utrecht University, The Netherlands*

---

## Abstract

Large earthquakes do not only heavily deform the crust in the vicinity of the fault, they also change the gravity field of the area affected by the earthquake due to mass redistribution in the upper layers of the Earth. Besides that, for sub-oceanic earthquakes deformation of the ocean floor causes relative sea level changes and mass redistribution of water that have again a significant effect on the gravity field. To model these deformations, sea level changes and gravity field perturbations self-consistently we use an adapted version of the sea level equation (SLE) that has been used for glacial isostatic adjustment studies. The sea level equation, next to our normal mode model for seismic solid earth modelling, allows us to compute a gravitationally self-consistent solution for the co-seismic relative sea level, surface deformation and geoid height changes. We apply our geographically detailed models to the case of the 2004 December 26 Sumatra-Andaman earthquake. Recent studies that have modelled the ocean mass effect on co-seismic gravity change for this specific earthquake show model results that indicate a broad negative change in geoid height around the fault due to ocean water redistribution [5], [13]. Our model results for the ocean contribution to geoid height differ from these studies in the sense that we find a pattern similar to the elongated dipole pattern of the solid earth model outputs for gravity and vertical deformation, together with a relatively small broad negative geoid height change. We explain the relation between outcomes for geoid height, relative sea level and vertical deformation of the ocean floor and we confront our model results with a least squares estimation of the co-seismic discontinuity in GRACE-derived gravity field time series. We show that taking into account the contribution of ocean water redistribution to the co-seismic geoid height change next to a compressible solid earth model is essential to explain the predominant negative co-seismic geoid anomalies from the GRACE gravity field solutions. Besides, we introduce a detailed approach to modelling an earthquake in a normal mode model that better approximates realistic continuous slip on the fault plane than models that do not distribute slip with depth. To demonstrate the importance of the slip distribution we show the differences in outcomes for modelled geoid height and vertical deformation.

*Keywords:* crustal deformation, co-seismic sea level change, geoid anomalies, normal mode modelling, GRACE, 2004 Sumatra-Andaman earthquake, sea level equation

---

## 1. Introduction

Earthquakes can cause large crustal deformations in the vicinity of the fault, in the order of a few meters uplift or subsidence for the Sumatra-Andaman earthquake on December 26 2004 [24]. Since these deformations imply mass redistribution within the solid earth, an earthquake also affects the gravity potential, which has been observed for the Sumatra-Andaman earthquake in gravity measurements from the GRACE satellite mission [10, 3, 18, 11, 5]. However, when an earthquake occurs underneath an ocean it is also the interaction between deformation of the ocean floor and water in the ocean that affects deformation and especially gravity. Water is redistributed over the region around the fault by the changed bathymetry and the changed gravity field, and these water movements have large effects on the geoid height: up to 50% of the co-seismic solid earth effect, as we will show in this paper. Besides, the water

---

*Email address:* d.b.t.broerse@tudelft.nl (D.B.T. Broerse)

redistribution will change the loading on the ocean floor that causes the Earth to deform. Understanding of the interaction between sea level, solid earth deformations and the gravity field is of great use for estimating local sea level changes for coastal areas affected by earthquakes.

In this paper we study how the distribution of seismic slip with depth will affect the vertical deformation and geoid height that we obtain from solid earth models. Next, we examine in qualitative and quantitative terms how the co-seismic redistribution of ocean water will change the regional relative sea level, geoid height and vertical deformation of the crust. For this purpose we adapt the sea level equation (SLE) [9], which describes the relation between vertical deformation of the ocean floor, geoid height and relative sea level, for the seismic case.

We apply our solid earth and sea level models to the Sumatra-Andaman earthquake, one of the largest earthquakes ever recorded; magnitude estimates range from  $M_w = 9.1$  to  $M_w = 9.3$  [2, 28]. Observations of emerged coral microatolls, both from in situ observations and satellite imagery [14], show uplift and subsidence of coral reefs surrounding the Andaman and Nicobar islands and the Indonesian archipelago, as do SAR images of coastal areas [27]. However, these observations lack the spatial coverage needed to constrain models of sea level change. The GRACE satellite mission is producing monthly solutions of the Earth's gravity field [26] since the beginning of 2002, hence this time-variable gravity field solution contains information on the co-seismic change of the geoid height for this earthquake. While the spatial resolution of the GRACE gravity model is limited, down to roughly 400 km [26] and errors increase at smaller wavelengths [29], it covers the complete area that is affected by the earthquake. Several recent studies have investigated the earthquake-related signals in the GRACE-derived data and found as co-seismic gravity change a dipole pattern where the negative pole east of the fault dominates over the positive pole west of the fault [3, 11, 5].

Two recently published studies present results for the ocean contribution in the co-seismic case: de Linage et al. [5] use a zeroth order approximation for the ocean contribution to the co-seismic geoid and gravity anomalies, and found a broad negative anomaly centered over the trench offshore. Melini et al. [13] present a full solution for the SLE but only show results for the change in relative sea level, where the ocean loading effect on the relative sea level is estimated as a broad sea level fall centered around the fault. We will compare our results with the aforementioned studies and investigate whether the ocean contribution to gravity is important in the comparison between model results and co-seismic changes in the GRACE-derived gravity field. Not only will we show that the ocean contribution to the co-seismic geoid height change is of the same order of magnitude as co-seismic solid earth effects, but also that the ocean contribution has a more detailed spatial pattern than previously published. Moreover, for the first time we explain the geophysical processes that cause the changes in relative sea level, geoid height and vertical deformation of the crust.

## 2. Co-seismic solid earth model for a shallow earthquake

Here we describe the model that we use to compute the elastic response caused by an earthquake, in terms of deformations and geoid height change. Subsequently, we describe how this specific type of model can be used to realistically model continuous seismic slip and how the distribution of slip with depth affects surface responses for shallow earthquakes with small dip angles in general. We use an analytic normal mode method for modelling the co-seismic surface deformations and geoid height changes [23], where the Earth is represented as a spherical, multi-layered, radially symmetric and self-gravitating body with a compressible elastic rheology [23].

The method makes use of point sources [19] and uses spherical harmonics to describe the surface responses. For a dip-slip fault with small dip angles ( $< 20^\circ$ ) the vertical deformation and geoid anomalies induced by a single point source are characterized by a pattern that has a positive peak next to a negative peak, which have a small scale with respect to the total width of a fault. To represent the actual continuous slip and to model the full saturated responses therefore a dense distribution of point sources is needed. Since the point sources that are distributed along the dip direction not only differ in depth but are shifted horizontally as well, we can expect the subsidence caused by the shallowest source to be partly counteracted by the uplift caused by the next source in depth, see figure 1. This effect increases with smaller dip angles because then the horizontal shift for sources increases, requiring a smaller spacing between the subsequent sources to obtain convergence. For clarity of the figure less point sources per unit depth are

shown than needed for convergence as the peaks of the subsequent individual profiles do not yet align.

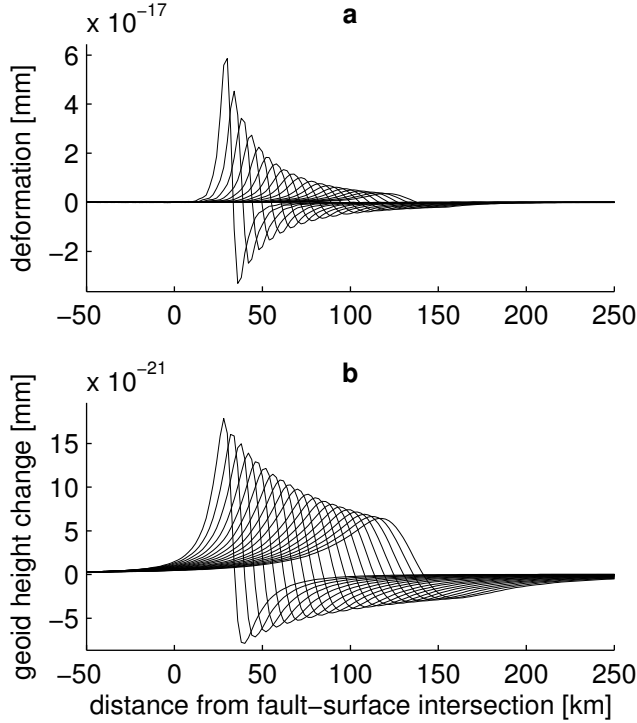


Figure 1: (a) The vertical deformation of the individual sources at successive depths on the fault plane in the dip direction. (b) Same as in a but for the geoid height change. As can be seen the surface response of one source is partially canceled by the other sources. The sources shown extend from 7 km depth (left) to 28 km depth (right) at a dip angle of  $12^\circ$ . All point sources have a seismic moment of 1 Nm. The crust parameters used are:  $\rho = 2200.00 \text{ kg/m}^3$ ,  $\mu = 0.620000 \cdot 10^{11} \text{ N/m}^2$ .

In literature, next to detailed slip models, models consisting of only a few point sources [13] and models with homogenous distribution of slip with depth [22, 15] have been used to model co-seismic vertical deformation or geoid changes. Therefore, to investigate the relevance of a realistic distribution of slip with depth we show in figure 2 the vertical deformation at the surface and the geoid height change due to three different 2D moment distributions as well as due to a single source at half the depth of the fault plane. The first two distributions (most moment release at halfway the fault and most moment release in the lower part of the fault) are typical for a dip slip fault and are similar to the moment with depth distributions of the slip model used in section 4. A point source and a homogenous distribution of seismic moment are used for comparison. All four distributions have a total seismic moment of 1 Nm and since a uniform rigidity is used at the depths of the fault the moment distribution is analogue to the slip distribution with depth. As can be seen in figure 2, with respect to models distributing slip over depth the co-seismic surface responses based on single depth models will differ in the following way: 1) maximum amplitudes increase; 2) the ratio between maximum positive and maximum negative increases; 3) the smaller wavelengths become more dominant; 4) locations of maximum amplitudes shift with respect to the fault. Hence the need for multiple point sources along the dip direction to model the continuous slip on the fault plane. Even at longer wavelengths models using single depths will deviate from models with slip distributed over depth (see figure 2).

More slip at lower depths will result in a larger negative deformation or geoid height change and more pronounced longer wavelengths. The effect is larger for vertical deformation than for the geoid as the vertical deformation response due to a single point source has a narrower pattern and the amplitude decreases faster with depth of the source. The geoid response has more power in the longer wavelengths and shows less decrease of amplitude with the depth of the source (compared to vertical deformation). This means that vertical deformation is more dependent on the distribution of moment or slip with depth than geoid height change.

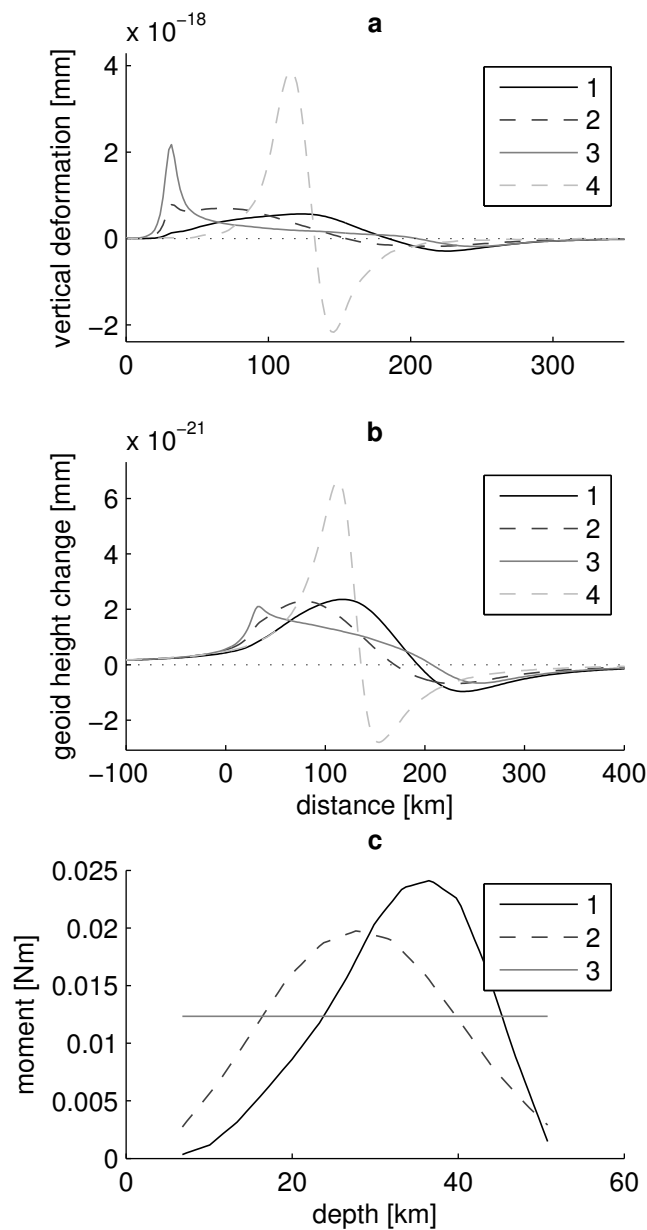


Figure 2: Solid earth responses to 4 different moment distributions with depth, of which the 2D distributions 1-3 are shown in subfigure c: uniform, one peaking at approximately half depth and one having most slip at lower depths, the fourth is a single point source halfway the 2D fault. All moment distributions have a total seismic moment of 1 Nm. (a) Cross-sections of vertical surface deformation using the moment distributions shown in c and the point source. (b) Same as a, but for geoid height change. All units are in mm.

### 3. Co-seismic sea level equation

The sea level equation (SLE), a solution for the change in relative sea level that is gravitationally self-consistent and includes the effect of solid earth deformation resulting from water mass redistribution, was proposed by Farrell and

Clark [9] for glacial isostatic adjustment (GIA), related to the accretion and melt of ice sheets. We can describe the relative sea level change as  $\Delta S(\theta, \phi)$  which is the geoid anomaly  $G(\theta, \phi, \Delta S)$  minus the vertical deformation  $R(\theta, \phi, \Delta S)$  of the sea floor, where  $\theta$  is the co-latitude and  $\phi$  is longitude [17]. To ensure that the sea level is only given in the oceans, the ocean function  $C(\theta, \phi)$  is used which is 1 in the oceans and 0 on land. This leads to the SLE

$$\Delta S(\theta, \phi) = C(\theta, \phi) \left( G(\theta, \phi, \Delta S) - R(\theta, \phi, \Delta S) \right) \quad (1)$$

As the change in relative sea level induces solid earth deformations and gravity changes, due to changed water loading and water displacement, equation 1 is nonlinear. Therefore we solve the SLE iteratively.

We adapt the SLE to the seismic case by removing the terms related to ice mass that are normally included in the SLE for GIA studies. Next, we introduce to the geoid height change  $G$  and vertical deformation  $R$  an initial geoid height change  $G_0(\theta, \phi)$  and initial vertical deformation  $R_0(\theta, \phi)$  caused by co-seismic solid earth deformation (comparable to Melini et al. [13]).  $\Delta\Phi$  represents the change in mean sea level and conserves the total mass in the oceans [9]. Together with an elastic response to the water redistribution ( $G_{ocean}$  and  $R_{ocean}$ ) the SLE becomes

$$\Delta S(\theta, \phi) = C(\theta, \phi) \left( G_0(\theta, \phi) + G_{ocean}(\theta, \phi, \Delta S) - R_0(\theta, \phi) - R_{ocean}(\theta, \phi, \Delta S) - \Delta\Phi \right) \quad (2)$$

in which

$$\Delta\Phi = 1/A_0 \int_{oceans} \Delta S dA \quad (3)$$

is the change in relative sea level integrated over the oceans divided by the total ocean area ( $A_0$ ).

We solve the SLE using a so-called pseudo-spectral algorithm, which means that the unmapped relative sea level change  $\Delta S L(\theta, \phi)$  is solved in the spectral domain up to high spherical harmonic degrees and the mapping on the ocean surface is performed in the spatial domain [17].

$$\Delta S L(\theta, \phi) = \sum_{l=0}^{\infty} \sum_{m=-l}^l \Delta S L_{lm} Y_{lm}(\theta, \phi) \quad (4)$$

where we substitute  $G_{ocean}$  and  $R_{ocean}$  in the manner of Mitrovica et al. [16]

$$\Delta S L_{lm} = \left( G_{0lm} - R_{0lm} + \frac{4\pi R_e^2}{2l+1} \left( \Delta L_{lm} [N_l - \Gamma_l] \right) \right) \quad (5)$$

Here  $R_e$  is the Earth radius,  $Y_{lm}$  the fully normalized spherical harmonics,  $\Delta L$  represents the load function and  $N_l$  and  $\Gamma_l$  the (elastic) responses for geoid and vertical deformation due to a unit surface load [8] for harmonic degree  $l$ . Furthermore,

$$\Delta L_{lm} = \rho_w \Delta S_{lm} \quad (6)$$

$$N_l = \frac{R_e}{M_e} \left[ 1 + k_l^E \right] \quad (7)$$

$$\Gamma_l = \frac{R_e}{M_e} \left[ h_l^E \right] \quad (8)$$

in which  $M_e$  is the mass of the Earth,  $\rho_w$  the water density and  $k_l^E$  and  $h_l^E$  the elastic surface load Love numbers for gravitational potential and vertical deformation respectively.  $\Delta\Phi$  can be rewritten as

$$\Delta\Phi = \Delta S_{00} / C_{00} \quad (9)$$

As a last step the change in sea level is mapped on the oceans in the spatial domain

$$\Delta S(\theta, \phi) = C(\theta, \phi) \left( \Delta S L(\theta, \phi) - \Delta\Phi \right) \quad (10)$$

A first order approximation for  $\Delta S$  ( $\Delta S_0$ ) is obtained by taking equation 2 and inserting  $G_0$  and  $R_0$  that are obtained from the normal mode modelling and omitting the water loading effects on vertical deformation  $R_{ocean}$  and geoid  $G_{ocean}$ .

Next,  $G_{ocean}$  of equation 2 is divided in two parts, using equation 7, to show different second order effects in the geoid height changes due to either the self-gravitating changed water distribution or to the elastic response of the solid earth to the changed surface load.

$$G_{selfgrav_{lm}} = T_l \Delta L_{lm} \cdot 1 \quad (11)$$

$$G_{elastic_{lm}} = T_l \Delta L_{lm} \cdot k_l^E \quad (12)$$

$$T_l = \frac{4\pi R_e^3}{(2l+1)M_e} \quad (13)$$

#### 4. Application to the 2004 December 26 Sumatra-Andaman earthquake

The normal mode method mentioned in section 2 is used to model the solid earth responses due to the seismic slip, the vertical deformation of the sea floor  $R_0$  and the geoid height change  $G_0$ , which are consequently used as initial inputs for the sea level equation, as described in section 3.

The rheology used is compressible and elastic; properties of the solid earth are derived from PREM [6], see table 1. We use the slip distribution model of Chlieh et al. [4], which is based on near field and regional GPS measurements and in situ and remote observations of coral reef vertical motions. Based on our earth layering this slip model results in a total seismic moment of  $8.25 \cdot 10^{22}$  Nm. Because we use a 2 km thick ocean layer our solid earth model has a radius of 6369 km and we use a 2 km upward continuation to determine the geoid height change at sea level ( $R = 6371$  km). For shallow earthquakes the co-seismic response still has considerable power in the high harmonic degrees, so to obtain a saturated solution the spherical harmonic expansion should be truncated at high degrees (up to 12,000). We can compute the responses up to a spherical harmonic degree  $l_{max} = 450$  for a compressible rheology, because of numerical instability at higher degrees. This means that we cannot resolve a large part of the short wavelength signal in the responses of the individual point sources. We tested for the incompressible case what part of the signal is missing by comparing a solution truncated at  $l_{max} = 450$  with a fully saturated incompressible solution using the normal mode approximation method for high-degree harmonics developed by Riva and Vermeersen [21]. The saturated solution shows that due to the summation of the surface responses of the individual point sources that are distributed over different depths almost all of the shorter wavelength signal is lost. Because of that, maximum values of both geoid height change and vertical deformation differ less than 4% from the incompressible solution truncated at  $l_{max} = 450$ . This allows us to truncate at much lower spherical harmonic degrees.

The resulting vertical deformation and upward continued geoid anomaly fields are subsequently used as input ( $R_0(\theta, \phi)$  and  $G_0(\theta, \phi)$ ) in the SLE of equation 2 which we solve up to  $l_{max} = 450$  as well. To construct the ocean function  $C(\theta, \phi)$  we make use of the ETOPO1 topography database [1] that we resampled from a 4 minute grid. Since the largest co-seismic deformations and geoid height changes in the direction along the dip are within a small spatial band ( $\approx 1^\circ$  for vertical deformation) relative to the length of the fault it is necessary to solve the models on a grid that can resemble the main details of the deformation field, therefore we use a  $0.1^\circ \times 0.1^\circ$  regular grid.

#### 5. GRACE

As mentioned in the introduction the data from the GRACE satellite mission allows us to validate our geoid height model results. As there is data two years before the earthquake and 5 years after it is possible to isolate the co-seismic signature of the earthquake. Various methods have been published to deal with the longitudinal stripes that can be found in geoid height maps [25, 30, 12]. These filter methods however not only remove part of the noise at short wavelengths but also remove longitudinal patterns like that of the co-seismic geoid height change pattern of the Sumatra-Andaman earthquake. We therefore choose to use only a simple filtering to preserve the co-seismic imprint

and to obtain a first order estimate of the co-seismic discontinuity using linear least squares fitting. We simultaneously estimate a post-seismic linear trend, yearly periodic signals and the 161-day tidal S2 aliasing [20] that unfortunately peaks around the location of the fault. The only methods of filtering we use are the truncation of the spherical harmonics at  $l_{max} = 60$  and a Gaussian smoothing filter that is used to remove a large part of the noise and truncation artifacts in the GRACE gravity field.

We use the Release 4 CSR and GFZ solutions for the GRACE Level-2 data for our analysis and apply the least squares estimation for individual points of a  $0.5^\circ$  by  $0.5^\circ$  grid. All gravity data is downward continued to a radius of 6371 km. The data we include in our analysis starts at February 2003 and ends at April 2010 with the exception of June 2003 (CSR solutions) or June 2003 and January as well as September 2004 (GFZ solutions). Of all individual monthly solutions we remove the average over the used period. The following equation is used to fit the time series of the geoid height

$$y = a \cdot \cos(2\pi t) + b \cdot \sin(2\pi t) + c \cdot \cos(2\pi\omega t) + d \cdot \sin(2\pi\omega t) + \begin{cases} e & \text{if } t < t_{eq} \\ f + g(t - t_{eq}) & \text{if } t \geq t_{eq} \end{cases} \quad (14)$$

where  $a$  to  $g$  are constants,  $\omega$  is 161/365, the 161-day S2 tidal alias phase,  $t$  the time in years and  $t_{eq}$  the time of the earthquake.

## 6. Results and discussion

### 6.1. Normal mode model results

Our normal mode model shows for both co-seismic vertical deformation ( $R_0$ ) and geoid height change ( $G_0$ ) an elongated dipole pattern of which the maximum positive is just east of the trench and maximum negative is located further east (figure 3a and b), which is a typical pattern for an earthquake with mainly dip-slip. Patterns for both  $R_0$  and  $G_0$  are similar, yet the geoid is more pronounced at larger wavelengths than the deformation. Without taking the sea level equation (SLE) into account our modelled vertical deformations lie between -2.7 and 5.2 m and geoid height change between -12.3 and 27.2 mm.

### 6.2. Combined solid earth and SLE results

Figure 3c and d show the combined model results of both co-seismic normal mode model and application of the SLE. The contribution of the SLE to the vertical deformation and geoid is depicted in figure 3e and f. The maximum effect of the SLE on the vertical deformation ( $R_{ocean}$ ) is between -9.1 and 35.0 mm, on the geoid ( $G_{ocean}$ ) between -12.9 and 1.6 mm. This results in a total co-seismic vertical deformation between -2.7 and 5.2 m and geoid height change between -10.9 and 14.2 mm. The co-seismic change in RSL,  $\Delta S$ , is between 5.2 and -2.7 m (figure 4a), which is the negative of the vertical deformation ( $R_0$ ) maxima, recalling that the RSL is geoid height minus vertical deformation, see equation 1. Since the vertical deformation input is two orders of magnitude larger than the geoid height change it causes the RSL mainly to be determined by the change in bathymetry.

We now consider the SLE contribution to the surface deformation  $R_{ocean}$ ; there where the ocean floor pushes away water due to uplift, the water column that loads the ocean floor decreases. This allows the ocean floor to react elastically, causing extra uplift. Conversely, at those locations where the ocean floor was already subsiding due to the earthquake, the water column will become higher which leads to extra subsidence. This result is shown in figure 3e, where we can also see that this effect is causing at maximum 35.0 mm uplift which is small compared to the direct (solid earth) effect of the earthquake.

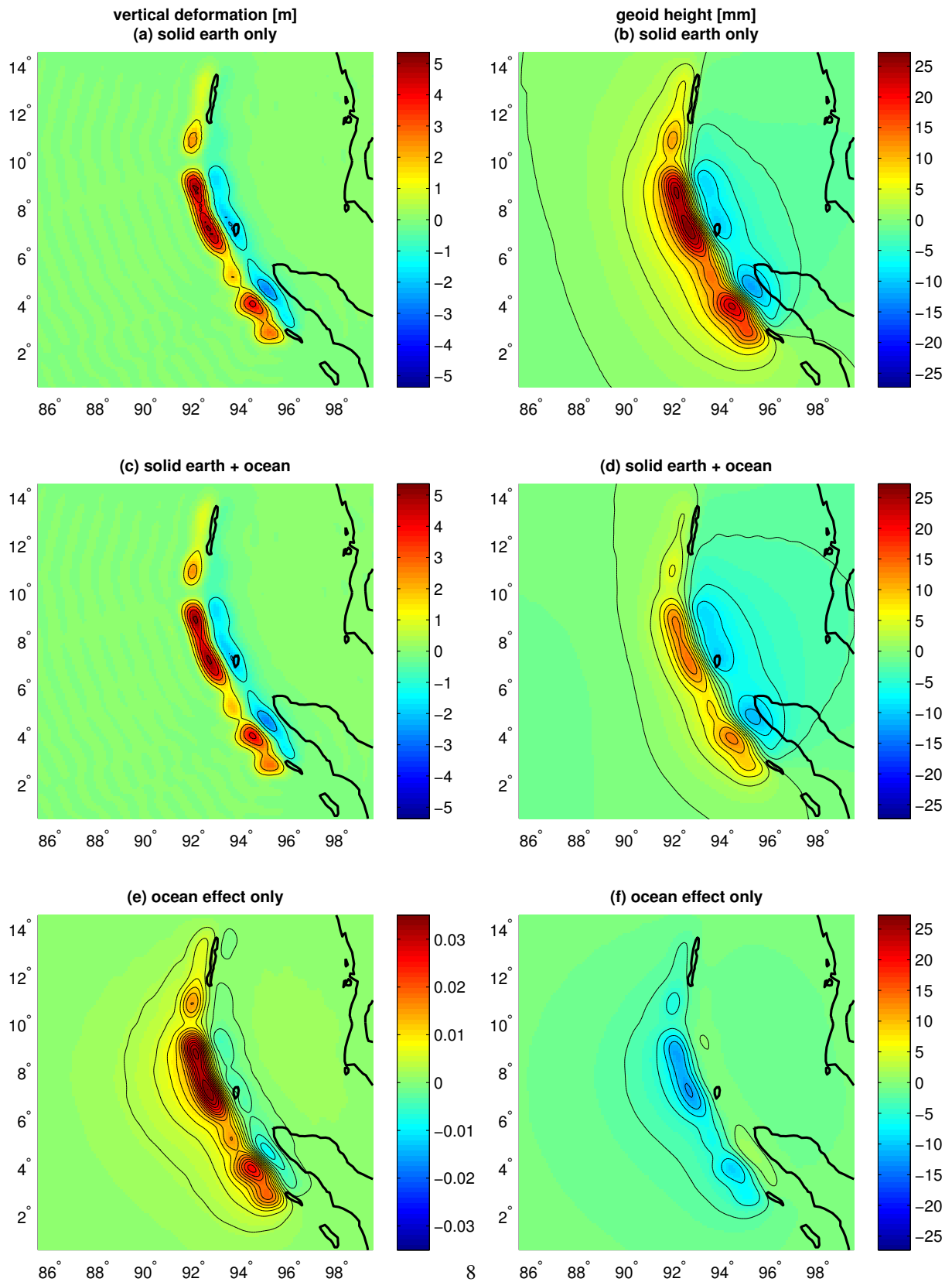


Figure 3: Solutions of normal mode model and sea-level equation due to the co-seismic fault slip. All deformations are in meters, geoid in mm. (a) Solid earth induced vertical deformation of the crust before application of the SLE,  $R_0$ . (b) Solid earth induced geoid height change before application of the SLE,  $G_0$ . (c) Solid earth and ocean water redistribution induced vertical deformation of the crust,  $R_0 + R_{ocean}$ . (d) Solid earth and ocean water redistribution induced geoid height change,  $G_0 + G_{ocean}$ . (e) Ocean water redistribution effect only on vertical deformation of the crust,  $R_{ocean}$ . Note the different color scale. (f) Ocean water redistribution effect only on geoid height change,  $G_{ocean}$ .

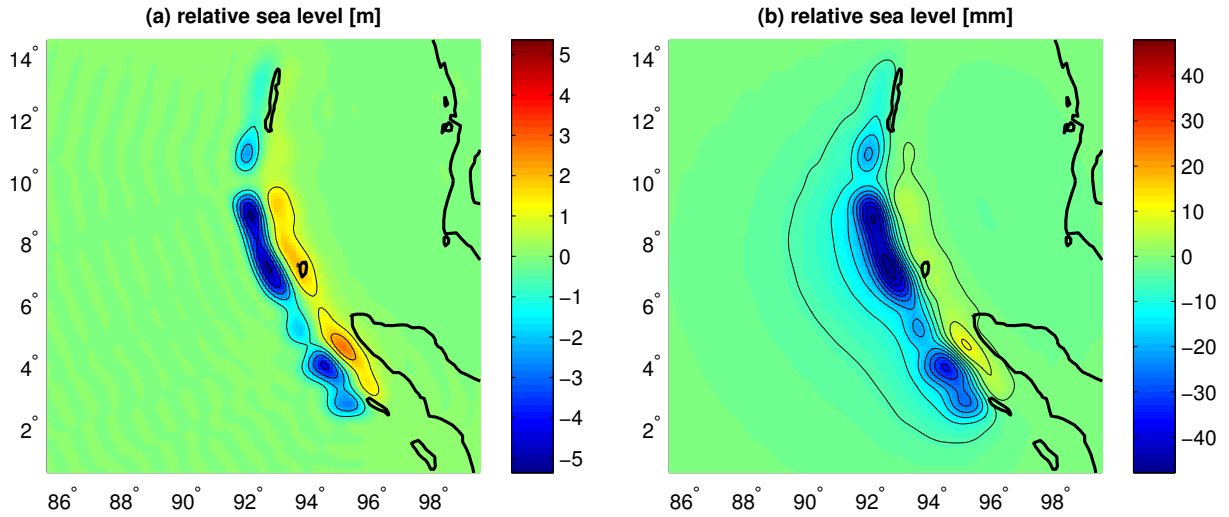


Figure 4: Relative sea level change in meters. (a) Relative sea level change after application of the SLE,  $\Delta S$ . (b) The converged relative sea level  $\Delta S$  minus the first order approximation of the relative sea-level change,  $\Delta S_0$ :  $\Delta S_{ocean}$ . Note the different scales.

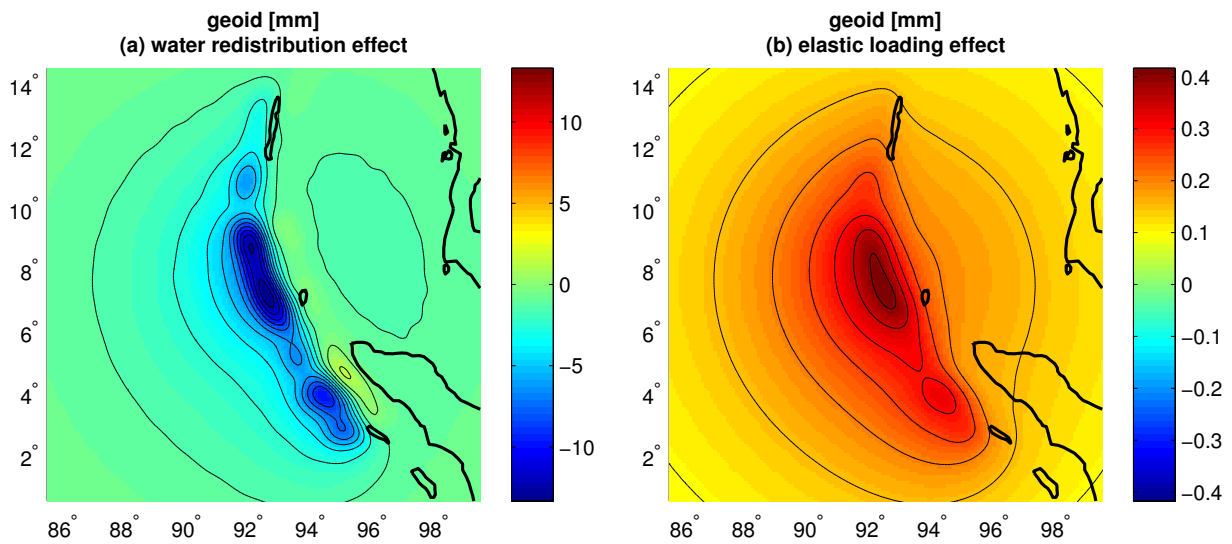


Figure 5: The results of ocean effect split up in two parts: (a) the change in geoid height due to redistribution of water mass that is mainly caused by bathymetry changes,  $G_{selfgrav}$ ; (b) the change in geoid height due to solid earth deformations caused by the changed water load on the crust,  $G_{elastic}$ .

The ocean mass redistribution effect on the geoid height,  $G_{ocean}$ , is divided in the gravity effect of redistributed water mass  $G_{selfgrav}$  (figure 5a) and the effect of the elastic deformation of the ocean floor due to changed loading,  $G_{elastic}$  (figure 5b). The first effect has a pattern that again corresponds to the typical dipole but with the negative anomaly west of the fault (where there is a RSL fall) and the positive anomaly east of the trench (where there is a RSL rise), so comparable to  $G_0$  (figure 3b) but of opposite sign. However, a broad negative geoid anomaly is clearly discernible as well in  $G_{selfgrav}$ , which is not visible at first sight in either the  $G_0$  and  $R_0$  SLE inputs (see figure 3). Since  $G_{selfgrav}$  is to the largest extent dependent on  $R_0$ , long-wavelength signals in the solid earth induced vertical deformation have to be examined. In figure 6 the vertical deformation is shown up to spherical harmonic degree 30, so that only long-wavelength patterns remain for  $R_0$ . In this figure only uplift is visible, which is pushing away water over a large area surrounding the fault, which in turn causes a long-wavelength negative geoid anomaly. This exclusively positive pattern is absent in the vertical deformation when using an incompressible model, where even at long wavelengths a dipole pattern remains.

$G_{elastic}$  only has a positive geoid anomaly west of the fault (related to the elastic uplift  $R_{ocean}$ ) and is smoother and around 30 times smaller than  $G_{selfgrav}$ . Adding the SLE effect to the normal mode results shows that the ocean has a large diminishing effect on geoid height change, primarily due to redistribution of water mass. Nevertheless, the strength of this diminishing effect is not necessarily the same for positive and negative geoid height changes, since it depends on the vertical deformation of the ocean floor. Next, instead of a diminishing effect, the long-wavelength uplift of the ocean floor causes a broad negative effect to the geoid height.

Two recent studies include the ocean mass redistribution effect on gravity, namely de Linage et al. [5], who use a zeroth order approximation to the ocean contribution on the geoid height, and Melini et al. [13] who use the full seismic SLE. de Linage et al. [5] show the contribution of ocean mass redistribution to gravity for the Sumatra-Andaman earthquake as a single spherical negative geoid or gravity anomaly over the trench. Melini et al. [13] do not show the SLE contribution to the geoid but confirm a geoid height change with the same sign and spatial extension as de Linage et al. [5]. Neither mentioned studies show features in ocean induced geoid anomalies or ocean loading induced relative sea level changes with smaller wavelengths that resemble the dipole patterns seen in the direct solid earth inputs ( $R_0$  and  $G_0$ ). For the long wavelengths we find an ocean induced negative geoid anomaly such as reported by the previously mentioned authors. However, for the first time we explain that this negative geoid anomaly is driven by the ocean response to a broad uplift of the ocean floor.

For the direct change in RSL ( $\Delta S_0$ ) we find a comparable pattern as Melini et al. [13], however our result is more pronounced in smaller wavelengths, probably because we used a higher maximum spherical harmonic degree. The second order effect of the ocean water redistribution on the RSL ( $\Delta S_{ocean}$ ), which is the converged RSL ( $\Delta S$ ) minus the first order approximation ( $\Delta S_0$ ), is displayed in figure 4b. This effect is mainly determined by  $G_{ocean}$  and  $R_{ocean}$ , leading to a dipole pattern, with the negative pole west of the trench (from a positive  $R_{ocean}$  and negative  $G_{ocean}$ ) and the positive pole east of the trench (from a negative  $R_{ocean}$  and positive  $G_{ocean}$ ). The range of  $\Delta S_{ocean}$  is between -47.9 mm and 10.7 mm, a small contribution to the total change in RSL. This is in contrast to the findings of Melini et al. [13], who find that the loading effect on RSL,  $\Delta S_{ocean}$ , has the form of a broad sea level fall with a maximum magnitude roughly 20% of the maximum magnitude of  $\Delta S_0$ . In our view this can only be caused by a large broad uplift of the sea floor due to changed water column,  $R_{ocean}$  or a large broad negative geoid anomaly  $G_{ocean}$ . While we do find a broad uplift pattern in  $R_0$ , we cannot explain the large magnitude using our elastic model. Possible explanations for both the broad negative relative sea level fall due to ocean loading and geoid height change due to ocean water redistribution of Melini et al. [13] could be: 1) a too simple slip model that leads to a too high estimate of the vertical deformation of the sea floor; 2) truncation at a low spherical harmonic degree that leads to a misrepresentation of all patterns in the interaction between geoid height, vertical deformation and relative sea level.

Concluding, for vertical deformation the application of the SLE implies a slight amplification of the original input pattern. This effect is however very small and probably not discernible in observation data, as the maximum amplitude changes by less than 1%. Also the first order approximation for the RSL ( $\Delta S_0$ ) is for the co-seismic case already a good enough approximation (within 99% of the final result). Yet, the ocean water redistribution effect on geoid height is far from negligible as the SLE reduces the co-seismic signature of the solid earth-only model and adds extra (negative)

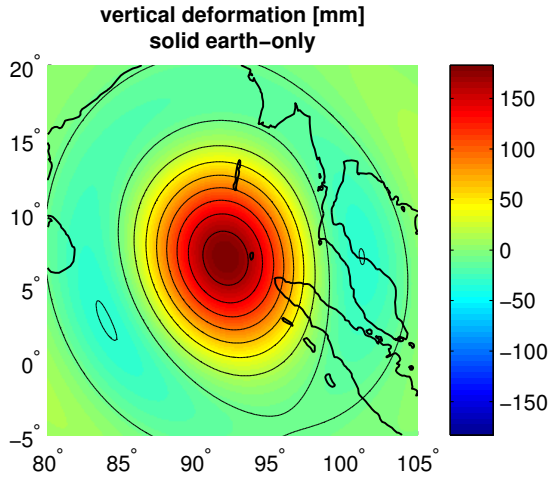


Figure 6: Vertical deformation, solid earth-only, truncated at spherical harmonic degree 30.

patterns related to a broad ocean floor uplift. In our case the positive geoid anomaly decreases by approximately 50% and the negative 10%. The choice of the earth parameters, like rigidity and density, only has a small influence on the contribution of the SLE on the geoid height as the elastic part,  $G_{elastic}$ , is very small.

### 6.3. Comparison with GRACE

The results of the least squares estimation of the co-seismic discontinuity in the time series of the GRACE gravity field are depicted in figure 7. Gaussian smoothing with a 200 km radius has been applied to remove most of the noise in the shorter wavelengths. These solutions show comparable patterns with a clear dipole where the positive pole appears west of the trench and the negative pole east of the trench. Using larger smoothing radii leads to removing mainly the positive pole that manifests more at smaller wavelengths than the negative pole. We find values for the maximum positive and negative geoid anomalies of -6.7 / 2.0 mm (CSR) and -6.8 / 2.4 mm (GFZ).

To be able to compare our modelled co-seismic geoid height change with the estimated GRACE co-seismic discontinuities we truncate our results at  $l_{max} = 60$  and apply the same Gaussian filtering as to the GRACE data. In figure 8a the modelled solid earth-only co-seismic geoid height change is displayed, showing a smoothed dipole with a dominant positive pole. The magnitude varies from -3.2 to 5.4 mm. In figure 8b the combined model result of solid earth and ocean contribution to geoid height is shown, ranging between -4.3 to 1.8 mm. While at short wavelengths the maximum amplitude of both negative and positive pole decreases after application of the SLE, at the long wavelengths only the positive pole decreases in magnitude and the negative pole even increases. In the electronic supplement we have added the same results, both for our model and GRACE, expressed as gravity anomalies.

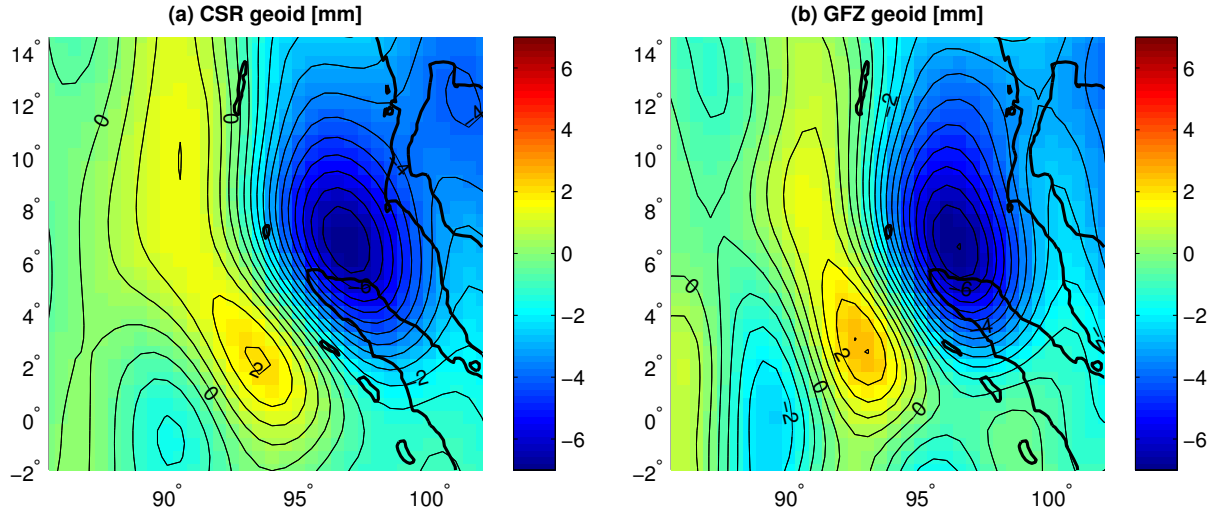


Figure 7: Co-seismic discontinuity estimated from GRACE-derived gravity models. (a) The estimated co-seismic discontinuities in geoid height using the CSR GRACE solutions, (b) idem, using the GFZ GRACE solutions. A Gaussian smoothing radius of 200 km is applied. Units in mm.

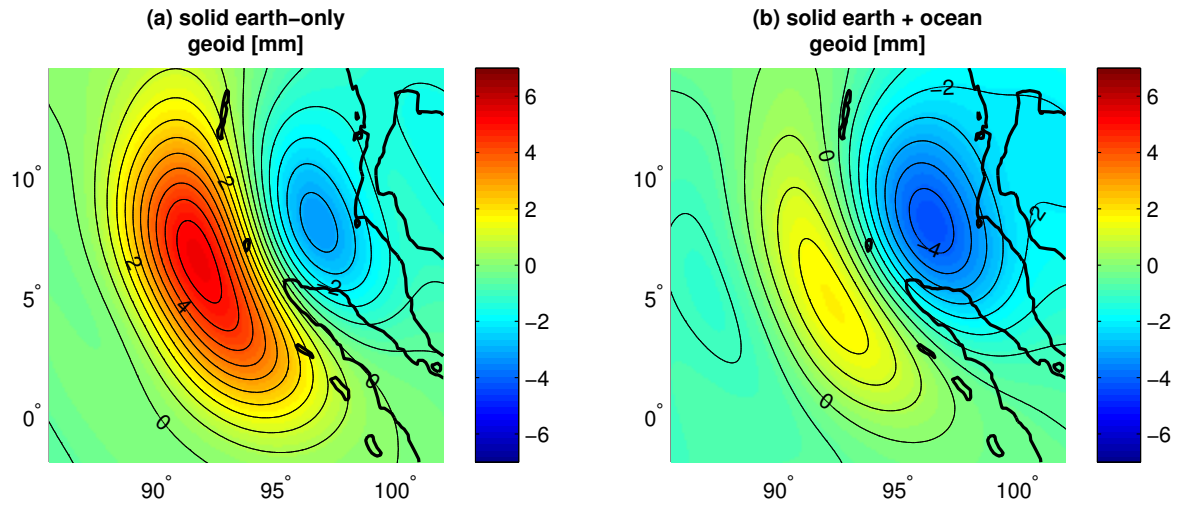


Figure 8: Model results truncated at maximum order and degree 60. (a) The modelled co-seismic discontinuity using a solid earth-only model. (b) Results for the combined model: solid earth and ocean loading induced discontinuities. A 200 km radius Gaussian smoothing is applied. Units in mm.

We obtain a good agreement between the co-seismic discontinuities estimated from GRACE and our model after application of the sea level equation, see figures 7 and 8. At  $l_{max} = 60$  the smoothed geoid has around the same ratio between maximum negative and positive magnitudes for both model and GRACE (2.5:1). Our model shows at  $l_{max} = 60$  on average a 30% smaller maximum magnitude for both poles than the GRACE estimate. Given the uncertainties in the slip model this is a good agreement. However, it must be noted that the GRACE estimates can be contaminated by noise and non-linearities of the real post-seismic trend. The location of the poles does agree relatively well, however our model results show the peak of the positive pole slightly more northward and the power in

the positive pole is distributed over a more elongated pattern compared to the GRACE estimates. Combined with the overall smaller amplitudes in the model this might suggest that with respect to the slip model used GRACE indicates more slip in the southern part of the fault.

Using the GRACE gravity observations, previous studies found a stronger negative anomaly than positive geoid anomaly for the Sumatra-Andaman earthquake as well [18, 5, 3, 11]. Some studies have also used models to explain the GRACE observations, e.g. [10, 5, 22]. The last two modelled the solid earth only geoid height change as a dipole with a more prominent positive anomaly than negative anomaly, but as already mentioned de Linage et al. [5] used a zeroth order approximation of the ocean effect and so obtained a more prominent negative pole. Han et al. [10] suggested that the effect of dilatation of the crust and mantle on gravity anomalies alone could explain an overall more negative co-seismic discontinuity. Our results for the co-seismic geoid anomalies imply that solely the ocean contribution or solely compressibility effects cannot give agreement between solid earth models and GRACE derived observations. However, only the interaction between ocean mass redistribution and low degree uplift of the ocean floor, which is only obtained using a compressible model, can cause a broad negative geoid anomaly superposed on the dominantly positive dipole caused by dip-slip.

## 7. Conclusions

For the normal mode model we have shown that the slip needs to be properly distributed over depth to approximate continuous seismic slip. The magnitude of both vertical surface deformation and geoid height change will be overestimated when using single depth point source models (e.g. the five point model from Tsai et al. [28]), resulting in an overestimation of the ocean water distribution effect on geoid height.

Our main conclusion regarding the co-seismic ocean contribution is that it has a small impact on crustal deformations and relative sea level but it alters significantly the geoid height with respect to the solid earth model. The positive anomaly is diminished by the SLE by 50% and the negative anomaly by 10%. Next, we showed that a broad uplift of the ocean floor causes a long-wavelength negative geoid anomaly. The spatial patterns of the ocean effect on co-seismic geoid height that we found are similar for the long wavelengths compared to those published recently by other authors; namely a broad negative geoid anomaly. However, we also found a short-wavelength dipole pattern in the ocean contribution to the geoid and relative sea level change. We explain for the first time the strong spatial dependence between patterns and magnitudes of the co-seismic vertical deformation and the ocean effect on geoid height.

We reach a good fit between the GRACE solutions and model for co-seismic geoid change if we take into account both compressibility of the crust and mantle next to the ocean mass redistribution. The ratio between the magnitude of the negative and positive parts of the dipole of our model agrees with the GRACE estimate, our amplitudes are only 30% smaller. Since the GRACE gravity field is truncated at a low spherical harmonic degree it cannot sample the high frequency features that make up most of the co-seismic gravity field. This can be seen in our model results where at different maximum spherical harmonic degrees ( $l_{max} = 450$ , see figure 3d or  $l_{max} = 60$ , see figure 8b) different ratios between positive and negative pole appear. Moreover, it should be noted that the GRACE gravity fields have a 1-month sampling, which means that in the time window between the actual earthquake and in the months after the earthquake processes that affect the gravity field, such as poro-elastic rebound and aftershocks, cannot be separated from the purely co-seismic and secular post-seismic gravity changes. The Nias earthquake on 2005 March 28 potentially influences the co-seismic signal estimated from GRACE, however this contribution is very difficult to separate from the Sumatra-Andaman earthquake contribution as shown by Einarsson et al. [7].

The SLE is an appropriate and complete approach to model the ocean response to co-seismic bathymetry and gravity changes, as it gives a gravitationally self-consistent solution for vertical deformation, geoid height change and relative sea level. Also, it is able to cope with the boundaries between sea and land area. Ocean water redistribution leads to an observable reduction and changed patterns of the geoid height at the spatial resolution of the GRACE gravity field. Therefore, for modelling gravity changes related to sub-oceanic earthquakes the contribution of ocean mass redistribution to gravity cannot be neglected.

## 8. Acknowledgments

The authors acknowledge financial support from ISES (D.B.T. Broerse), TOPO-EUROPE (W. van der Wal) and the NWO/SRON grant GO-AO/20 (R. Riva). Furthermore we want to thank the anonymous reviewers for their reviews and Bert Wouters and Ernst Schrama for their comments.

## 9. References

- [1] Amante, C., Eakins, B., 2008. ETOPO1 1 arc-minute global relief model: procedures, data sources and analysis. National Geophysical Data Centre, NESDIS, NOAA, US Department of Commerce, Boulder.
- [2] Ammon, C., Ji, C., Thio, H., Robinson, D., Ni, S., Hjorleifsdottir, V., Kanamori, H., Lay, T., Das, S., Helmberger, D., Ichinose, G., Polet, J., Wald, D., 2005. Rupture process of the 2004 Sumatra-Andaman earthquake. *Science* 308 (5725), 1133–1139.
- [3] Chen, J., Wilson, C., Tapley, B., Grand, S., 2007. GRACE detects coseismic and postseismic deformation from the Sumatra-Andaman earthquake. *Geophys. Res. Lett.* 34, L13302.
- [4] Chlieh, M., Avouac, J., Hjorleifsdottir, V., Song, T., Ji, C., Sieh, K., Sladen, A., Hebert, H., Prawirodirdjo, L., Bock, Y., Galetzka, J., 2007. Coseismic slip and afterslip of the great Mw 9.15 Sumatra-Andaman earthquake of 2004. *Bull. Seismol. Soc. Am.* 97 (1A), S152–S173.
- [5] de Linage, C., Rivera, L., Hinderer, J., Boy, J., Rogister, Y., Lambotte, S., Biancale, R., 2009. Separation of coseismic and postseismic gravity changes for the 2004 Sumatra-Andaman earthquake from 4.6 yr of GRACE observations and modelling of the coseismic change by normal-modes summation. *Geophys. J. Int.* 176 (3), 695–714.
- [6] Dziewonski, A., Anderson, D., 1981. Preliminary reference Earth model. *Phys. Earth Planet. Inter.* 25 (4), 297–356.
- [7] Einarsson, I., Hoechner, A., Wang, R., Kusche, J., 2010. Gravity changes due to the Sumatra-Andaman and Nias earthquakes as detected by the GRACE satellites: a reexamination. *Geophys. J. Int.* 183 (2), 733–747.
- [8] Farrell, W., 1972. Deformation of the Earth by surface loads. *Rev. Geophys.* 10 (3), 761–797.
- [9] Farrell, W., Clark, J., 1976. On postglacial sea level. *Geophys. J. Int.* 46, 647–667.
- [10] Han, S., Shum, C., Bevis, M., Ji, C., Kuo, C., 2006. Crustal dilatation observed by GRACE after the 2004 Sumatra-Andaman earthquake. *Science* 313 (5787), 658–662.
- [11] Han, S., Simons, F., 2008. Spatiospectral localization of global geopotential fields from the Gravity Recovery and Climate Experiment (GRACE) reveals the coseismic gravity change owing to the 2004 Sumatra-Andaman earthquake. *J. Geophys. Res.* 113 (B1), B01405.
- [12] Klees, R., Revtova, E., Gunter, B., Ditmar, P., Oudman, E., Winsemius, H., Savenije, H., 2008. The design of an optimal filter for monthly GRACE gravity models. *Geophys. J. Int.* 175 (2), 417–432.
- [13] Melini, D., Spada, G., Piersanti, A., 2010. A sea level equation for seismic perturbations. *Geophys. J. Int.* 180 (1), 88–100.
- [14] Meltzner, A., Sieh, K., Abrams, M., Agnew, D., Hudnut, K., Avouac, J., Natawidjaja, D., 2006. Uplift and subsidence associated with the great Aceh-Andaman earthquake of 2004. *J. Geophys. Res.* 111, B02407.
- [15] Migliaccio, F., Reguzzoni, M., Sansò, F., Via, G.D., Sabadini, R., 2008. Detecting geophysical signals in gravity satellite missions. *Geophys. J. Int.* 172 (1), 56–66.
- [16] Mitrovica, J., Davis, J., Shapiro, I., 1994. A spectral formalism for computing three-dimensional deformations due to surface loads 1. Theory. *Journal of Geophysical Research* 99 (B4), 7057–7073.
- [17] Mitrovica, J., Peltier, W., 1991. On postglacial geoid subsidence over the equatorial oceans. *J. Geophys. Res.* 96 (B12), 20053–20071.
- [18] Panet, I., Mikhailov, V., Diament, M., Pollitz, F., King, G., de Viron, O., Holschneider, M., Biancale, R., Lemoine, J., 2007. Coseismic and post-seismic signatures of the Sumatra 2004 December and 2005 March earthquakes in GRACE satellite gravity. *Geophys. J. Int.* 171 (1), 177–190.
- [19] Piersanti, A., Spada, G., Sabadini, R., 1997. Global postseismic rebound of a viscoelastic Earth: Theory for finite faults and application to the 1964 Alaska earthquake. *J. Geophys. Res.* 102, 477–492.
- [20] Ray, R., Luthcke, S., 2006. Tide model errors and GRACE gravimetry: towards a more realistic assessment. *Geophys. J. Int.* 167 (3), 1055–1059.
- [21] Riva, R., Vermeersen, L., 2002. Approximation method for high-degree harmonics in normal mode modelling. *Geophys. J. Int.* 151 (1), 309–313.
- [22] Sabadini, R., Dalla Via, G., Hoogland, M., Aoudia, A., 2005. A splash in Earth gravity from the 2004 Sumatra earthquake. *Eos Trans. AGU* 86 (15), 149–150.
- [23] Sabadini, R., Vermeersen, B., 2004. *Global Dynamics of the Earth: Applications of Normal Mode Relaxation Theory to Solid-Earth Geophysics*. Kluwer Acad., Dordrecht, Netherlands.
- [24] Subarya, C., Chlieh, M., Prawirodirdjo, L., Avouac, J., Bock, Y., Sieh, K., Meltzner, A., Natawidjaja, D., McCaffrey, R., 2006. Plate-boundary deformation associated with the great Sumatra–Andaman earthquake. *Nature* 440 (7080), 46–51.
- [25] Swenson, S., Wahr, J., 2006. Post-processing removal of correlated errors in GRACE data. *Geophys. Res. Lett.* 33 (8), L08402.
- [26] Tapley, B., Bettadpur, S., Watkins, M., Reigber, C., 2004. The gravity recovery and climate experiment: Mission overview and early results. *Geophys. Res. Lett.* 31 (9), L09607.
- [27] Tobita, M., Suito, H., Imakiire, T., Kato, M., Fujiwara, S., Murakami, M., 2006. Outline of vertical displacement of the 2004 and 2005 Sumatra earthquakes revealed by satellite radar imagery. *Earth Planets Space* 58 (12), e1–e4.
- [28] Tsai, V., Nettles, M., Ekström, G., Dziewonski, A., 2005. Multiple CMT source analysis of the 2004 Sumatra earthquake. *Geophys. Res. Lett.* 32, L17304.
- [29] Wahr, J., Swenson, S., Velicogna, I., 2006. Accuracy of GRACE mass estimates. *Geophys. Res. Lett.* 33 (6), L06401.
- [30] Wouters, B., Schrama, E., 2007. Improved accuracy of GRACE gravity solutions through empirical orthogonal function filtering of spherical harmonics. *Geophys. Res. Lett.* 34 (23), L23711.

## 10. Supplementary material

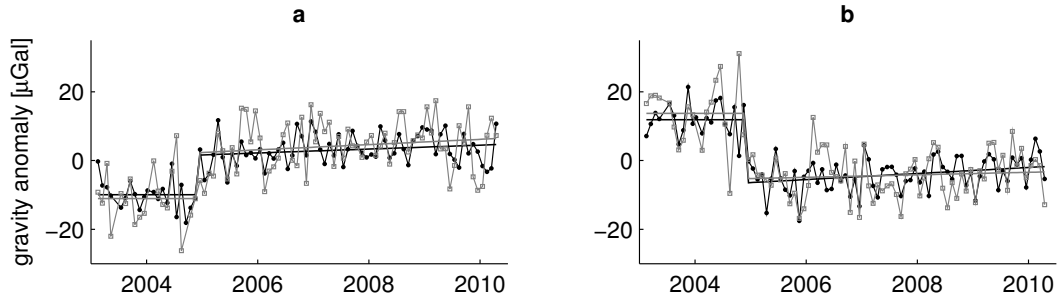


Figure 9: The gravity anomaly time series using the CSR (black) and GFZ (grey) solutions at two locations: (a)  $\text{lat}=2.5^\circ / \text{lon}=93.5^\circ$  where we found a maximum in the co-seismic discontinuity and (b)  $\text{lat}=6.5^\circ / \text{lon}=96.5^\circ$  where a co-seismic low in the geoid height change was found. These locations are highlighted with a cross in figure 7. The estimated linear fits, including co-seismic discontinuity and post-seismic linear trend, are displayed as well. A 250 km Gaussian smoothing radius has been applied to the time series.

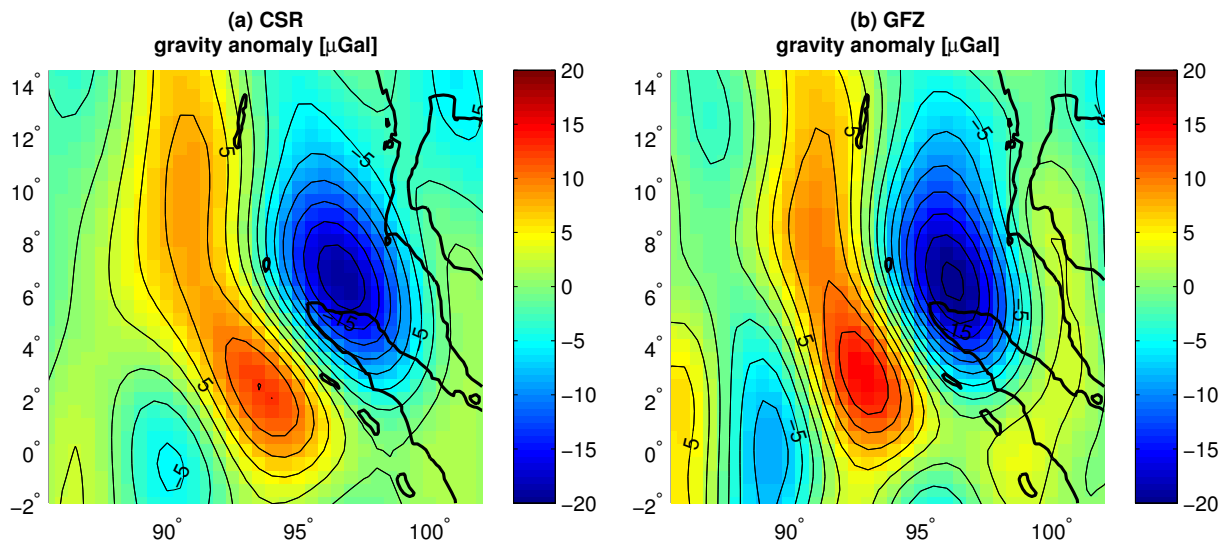


Figure 10: Co-seismic discontinuity estimated from GRACE-derived gravity models as gravity anomalies, using the GRACE gravity solutions of (a) CSR, and (b) GFZ. Analogue to the geoid height change we find a dipole, but with a more prominent magnitude of the positive pole relative to the magnitude of the negative pole. The positive pole appears to be mostly prominent in the smaller wavelengths and is therefore magnified in the gravity anomalies. Maximum values for the co-seismic gravity anomalies are found to be  $-18 / 12 \mu\text{Gal}$  (CSR) and  $-20 / 14 \mu\text{Gal}$  (GFZ) at a 250 km smoothing radius.

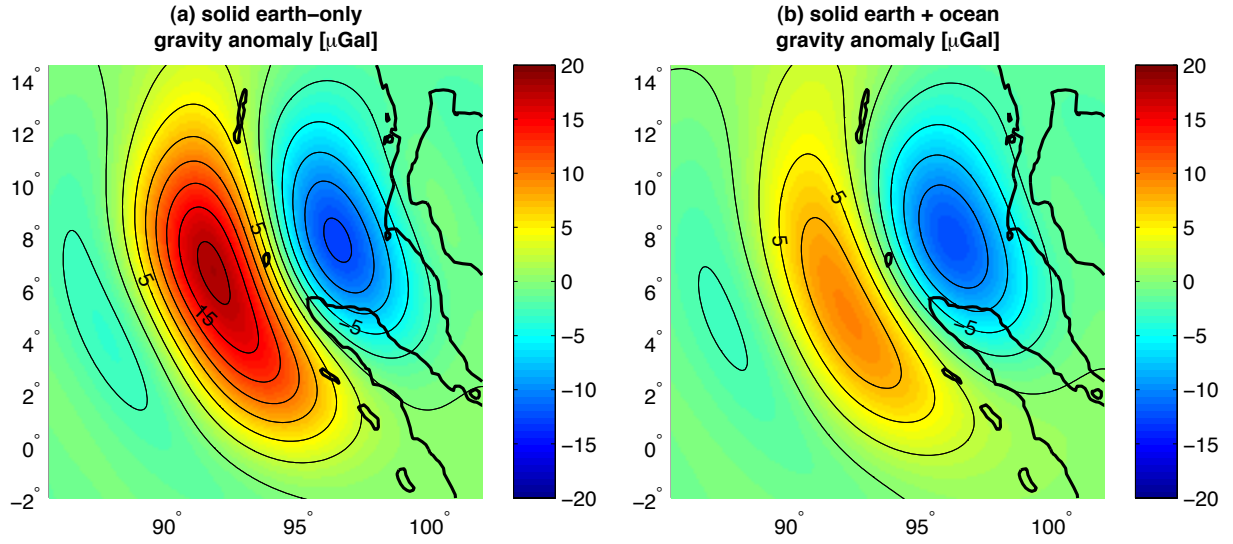


Figure 11: Model results truncated at maximum order and degree 60 and expressed as gravity anomalies. (a) The modelled co-seismic discontinuity using a solid earth-only model, with values between  $-13.0$  and  $18.2 \mu Gal$ . (b) Results for the combined model: solid earth and ocean loading induced discontinuities, with values between  $-12.4$  and  $9.5 \mu Gal$ . A 250 km Gaussian smoothing radius is applied.

layer	r [km]	$\rho[kg/m^3]$	$\mu[N/m^2]$	$\lambda[N/m^2]$
1	6369	2520.00	$0.341 \cdot 10^{11}$	$0.395 \cdot 10^{11}$
2	6347	3380.00	$0.677 \cdot 10^{11}$	$0.858 \cdot 10^{11}$
3	6311	3377.00	$0.673 \cdot 10^{11}$	$0.853 \cdot 10^{11}$
4	6291	3375.00	$0.646 \cdot 10^{11}$	$0.862 \cdot 10^{11}$
5	6256	3367.00	$0.637 \cdot 10^{11}$	$0.852 \cdot 10^{11}$
6	6151	3476.00	$0.747 \cdot 10^{11}$	$1.16 \cdot 10^{11}$
7	5971	3858.00	$1.04 \cdot 10^{11}$	$1.63 \cdot 10^{11}$
8	5701	4501.00	$1.75 \cdot 10^{11}$	$2.28 \cdot 10^{11}$
9	5200	4785.00	$2.07 \cdot 10^{11}$	$2.89 \cdot 10^{11}$
10	4700	5050.00	$2.36 \cdot 10^{11}$	$3.50 \cdot 10^{11}$
11	4200	5319.00	$2.66 \cdot 10^{11}$	$4.18 \cdot 10^{11}$
12	3630	5510.00	$2.88 \cdot 10^{11}$	$4.60 \cdot 10^{11}$
13	3480	10931.00	0	$9.42 \cdot 10^{11}$

Table 1: Parameters for the elastic earth model. r is the distance with respect to the center of the Earth,  $\rho$  is the density of the layer,  $\mu$  is the rigidity and  $\lambda$  the first Lamé parameter.